# Examination of high porosity activated carbon obtained from dehydration of white sugar for electrochemical capacitor applications

Kabir O. Oyedotun[1], Farshad Barzegar[2], Abdulmajid A. Mirghni[1], Abubakar A. Khaleed[1], Tshifhiwa M. Masikhwa[1], and Ncholu Manyala[1]*

[1]Department of Physics, Institute of Applied Materials, SARChI Chair in Carbon Technology and Materials, University of Pretoria, Crn Lynnwood and University Road, Hatfield, Pretoria 0002, South Africa.

[2] Department of Electrical, Electronic and Computer Engineering, University of Pretoria, University Road, Hatfield, Pretoria 0002, South Africa.

*Corresponding author's email: ncholu.manyala@up.ac.za, Tel.: + (27)12 420 3549.

## ABSTRACT

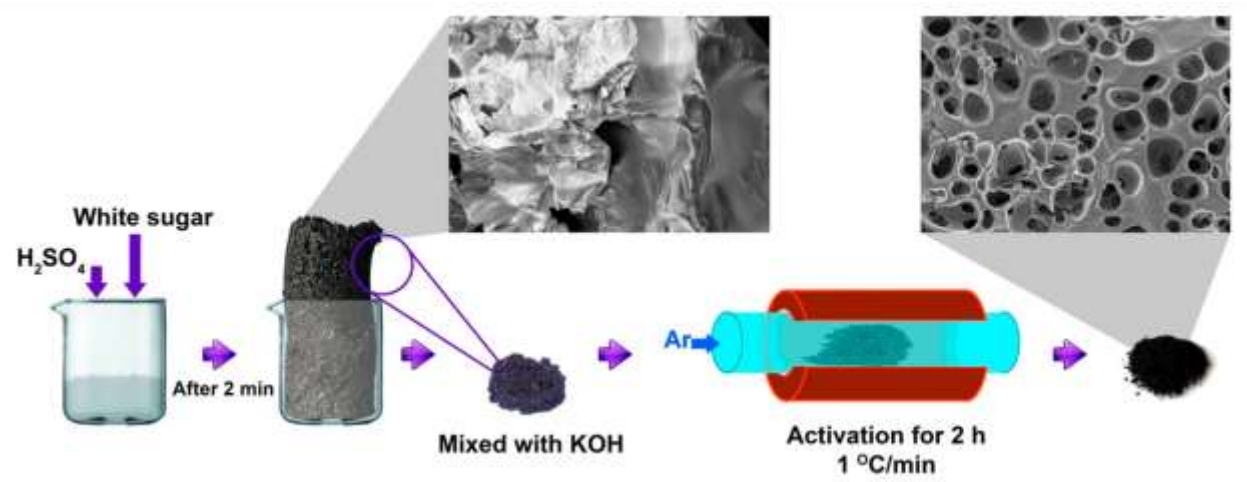


In this research study, we have presented a simple two-step synthesis path to producing a cost-effective high porosity carbon material via acidic dehydration of white sugar. The electrochemical behaviour of the activated sugar-based carbon material (ASC), activated at 400°C (ASC 400) and adopted as a supercapacitor electrode in a symmetric device demonstrated a limit specific capacitance of 242.67 F $g^{-1}$ at 1 A $g^{-1}$. The device also demonstrated a good efficacy as an established material for supercapacitors suitable for high power applications with a satisfactory energy density of 19 Wh $Kg^{-1}$ and power density, 750 W $kg^{-1}$ at a gravimetric specific current of 1 A $g^{-1}$. The results obtained provide

a potential route to converting cheap refined biomass sources into highly porous nanostructured materials for energy storage device applications.

**KEYWORDS:** Write sugar; carbonization; $Na_2SO_4$, specific capacitance; specific surface area; $H_2SO_4$.

## INTRODUCTION

Supercapacitors (SCs), described as prominent high power-delivery energy storage devices are known to store a lot more electrical charge than the conventional capacitors. They have received more research attentions in the energy storage applications owing to their ability to quickly and comfortably discharge the stored energy speedily, thus, producing the needed high power and extended cycle life in comparison to batteries. They are able to complement batteries in several areas of applications, such as domestic and industrial among others. SCs have the capability to work at very low temperatures, a unique quality that knocks down the choice of several types of batteries as a better device for energy applications [1-3,41-42].

SCs store charges electrostatically, unlike through reversible chemical reactions for rechargeable batteries. They can be discharged and recharged up to a very high number of cycles without losing their capacitance. The little or negligible internal resistance attribute of the SCs makes them store and dispense energy effortlessly, and work at an efficiency very close to a hundred percent [4-5]. The properties of SCs come from the intrinsic energy storage mechanism. Mostly, the combination of a suitable electrode material and the corresponding compatible electrolyte type largely determines the functionality, thermal and electrical characteristics of a supercapacitor. The numerous

merits present in SCs have made them take up the technologically developing markets ranging from applications in consumer electronics, power-back up/emergency units to electric/hybrid electric vehicles [6–9]. However, the energy density of SCs still requires an improvement compared to that of a battery, but their high power density gives them the edge in applications where a sharp incipient amount of current is needed owing to their instant discharge ability.

Recently, SCs are being employed in combination with batteries to lift their power supply capacity [10]. Nonetheless, various devices application in a single system is not the ultimate attempt owing to variations in individual cell properties such as capacitance, capacity and cycle life among others [11]. In order to fulfill the required high energy and power densities in a single device, hybrid supercapacitors that integrate the properties of the conventional supercapacitor with those of the lithium ion battery have been recently reported by different researchers in the literature [11-14]. The hybrid supercapacitor utilize one electrode with high lithium ion kinetics, and the other ( such as activated carbons) with high contact area with the electrolyte [12]. SCs are composed of two electrodes closely packed together and submerged in an electrolyte, which serves as the conducting medium between the electrodes. The electrodes in *SCs* are highly porous, giving them a much larger specific surface area, SSA than conventional capacitors. This increases the surface for charge storage resulting in improved device electrochemical performance [15].

Widely, numerous materials are adopted in study and fabrication of SCs electrodes [16-18]. However, the essential factors such as the electrical conductivity, form, cost-effectiveness and stability, can be achieved by adapting the material precursors. Research studies on carbon materials as SCs electrodes have yielded some exciting results in a number of studies [15]. These carbon materials include activated carbons from tree barks [9], biomass wastes [19–21], sugar cane [22,23] as well as refined sugar [24] to mention but a few.

Sugar, a common word for sweetened, short-chain and soluble carbohydrates is also regarded as readily available and cheap source of carbon. They are mostly utilized in foods that are made up of hydrogen, carbon, and oxygen. Sugars are derived from various sources. The simple sugars also referred to as monosaccharides include glucose or dextrose, fructose, and galactose. A "table sugar" or "granulated sugar" mostly employed as food is sucrose, which is a disaccharide of glucose and fructose [25,26]. Sugars can be extracted from the tissues of most plants.They are sufficiently obtainable in high concentrations solely in sugarcane [27].

Purified sugar can be obtained from raw sugar after undergoing a process to removing the molasses. The raw sugar, sucrose is extracted from sugarcane or sugar beet. The purifying process is to remove unpleasant tastes from the raw sugar, resulting in refined or white sugar [28].

There have been a few research outcomes on the adoption of sugar-derived carbons for applications such as energy storage devices. Wang X. et al. [29] reported highly conductive carbons with high specific surface area , synthesized using a sugar-blowing method to develop a 3D self-supported graphene referred to as strutted graphene. A device fabricated from the as-produced carbon demonstrated a gravimetric specific capacitance of 250 F $g^{-1}$ at a specific current of 1 A $g^{-1}$ and excellent stability using $H_2SO_4$ aqueous electrolyte. Similarly, Ma J. et al. [30] reported a composite material made up of sugar-derived carbon and graphene produced by mixing glucose with graphene oxide using ultra-sonication and calcination steps. The 3D composite material as electrodes for SCs displayed a high specific capacitance of about 273 F $g^{-1}$ at a specific current of 0.5 A $g^{-1}$, with excellent electrochemical stability in KOH electrolyte.

In this study, we report the commercial scale synthesis, chemical, microstructural and electrochemical characterization of as-prepared carbon via acidic dehydration of white sugar. The KOH activated carbon was obtained from the dehydrated carbon material through a cost-effective atmospheric pressure chemical vapour deposition (APCVD) technique at varying calcination temperatures. This technique holds great potential for its suitability in morphology control as well as pore-structure fine-tuning in solute phase. The electrochemical evaluations of a symmetric SC fabricated with the as-prepared carbon material were thereafter analyzed in 1 M $Na_2SO_4$ electrolyte. A specific analysis of the fabricated electrodes tested in both the three and two-electrode configurations revealed that a working potential of 1.5 V could be achieved for a symmetric ASC 400//ASC 400 electrochemical capacitor operating in 1 M $Na_2SO_4$ electrolyte. The fabricated carbon material was observed to be consistent within this potential with no environmental concern such as corrosion, resulting in high specific capacitance, good pore size distribution, and high energy and power densities among others, compared to some other similar materials in the literature. The KOH adopted as the activating agent was selected since it induces a well-defined distribution of micropores at low activation temperatures with high carbon throughputs [31,32].

## EXPERIMENTAL

### Material preparation

A stoichiometric amount of white sugar was poured in a glass beaker with a stoichiometric volume of $H_2SO_4$ (99.99 %) being poured onto it and then stirred for about 2 min. by magnetic stirrer at 25 °C. The reaction, which lasted for nearly 5 sec. was highly exothermic and resulted in the as-prepared carbon material (as shown in Scheme 1). The

following equation (1) below summarizes the reaction route to obtain the as-prepared ASC samples.

$$C_{12}H_{22}O_{11(s)} + 11H_2SO_{4(aq)} \rightarrow 12C_{(s)} + 11H_3O^{+}_{(aq)} + 11HSO^{-}_{4(aq)} \quad (1)$$

The obtained carbonized materials were washed severally using DI water and dried for 10 hours in an electric oven at a temperature of 60 °C in ambient condition. Afterwards, 1 g of the recovered carbon sample was muddled with 2 g of KOH and then put in an APCVD device at a ramping rate of 1 °C/min. for activation at temperatures of 400, 500, 600, and 700 °C respectively, for a dwelling time of 2 h in argon gas environment. The resulting carbon sample was soaked in 3 M HCl to remove any residual unreacted KOH before being washed severally using DI water and then dried overnight at 60 °C in ambient condition. The recovered products were designated as ASC 400, ASC 500, ASC 600 and ASC 700 in line with increasing activation temperatures respectively.

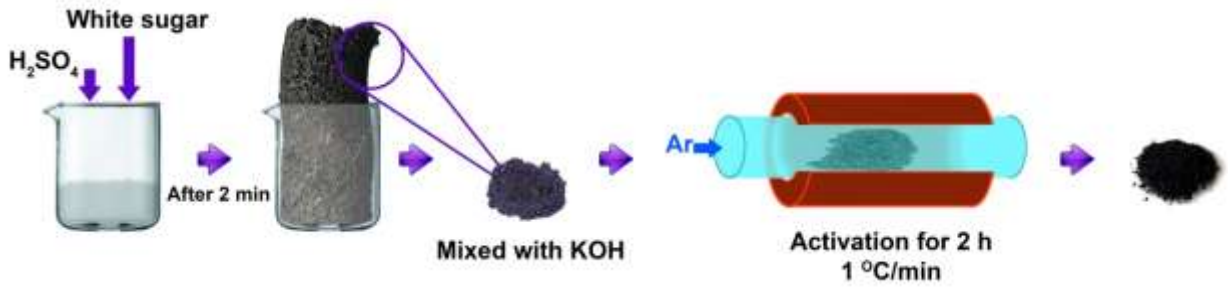


**Scheme 1.** Schematic of the synthesis route of ASC samples.

**Electrodes fabrication**

The as-prepared activated carbon electrodes were fabricated by making a blend of the active material (80 wt %), conductive carbon black (10 wt. %) and a polyvinylidene fluoride

(PVDF) (10 wt. %) binder, in a little drops of N-methyl-2-pyrrolidone (NMP) and stirred together to make up a homogeneous slurry. The prepared slurry was pasted on a 1 cm x 1 cm nickel foam used as current collector, and subsequently dried at 60 °C for about 10 h to remove NMP.

**Materials characterization**

Scanning electron microscopy and microanalysis were performed with the aid of a Zeiss Crossbeam 540 FEG-SEM, and a JEOL-2100F transmission electron microscope (TEM FEI Technai-F30) operating at an acceleration voltage of 200 kV. Phase identification was achieved by adopting a XPERT-PRO X-ray diffractometer (PANalytical BV, Netherlands) operating with a Cu Kα radiation source ($\lambda$ = 0.15418 nm). A Jobin–Yvon Horiba TX 6400 micro-Raman spectrometer operating with a 532 nm excitation laser was adopted for the Raman analysis. The pore size distribution and specific surface area of the samples were determined at -196 °C in liquid $N_2$ using a Micromeritics TriStar II 3020 system in a relative pressure ($P/P_0$) range of 0.01–1.0, alongside a model of Brunauer-Emmett-Teller (BET) and Barrett–Joyner–Halenda (BJH). All samples were degassed at 100 °C for 18 h in vacuum before absorption and desorption measurements.

**Electrochemical assessments**

The fabricated electrode was assessed with the help of a Bio-Logic VMP300 potentiostat (Knoxville TN 37,930, USA) under the influence of EC-Lab® V11.40 software. Every electrochemical assessment was done in a standard three-electrode set-up, with the

nickel-supported active material, glassy carbon and Ag/AgCl electrode selected as working electrode, counter electrode as well as reference electrode in 1 M $Na_2SO_4$ aqueous solution respectively. The specific mass of active material coated on every electrode was calculated to be nearly 3.2, 3.1, 3.0 and 3.2 mg $cm^{-2}$ for the ASC 400, ASC 500, ASC 600 and ASC 700 samples respectively. The electrochemical behavioural investigation of an assembled ASC 400 symmetric SC was performed using a standard two-electrode set-up in 1 M $Na_2SO_4$ solution. Cyclic voltammetry (CV), galvanostatic charge-discharge (GCD) as well as electrochemical impedance spectroscopy (EIS) of the sample were performed to observe the performance of the sample.

The specific capacitance ($C_s$) of the as-prepared single half-cell electrodes was evaluated in line with the equation below:

$$C_s = \frac{I \times \Delta t}{m \times \Delta V} \quad [F g^{-1}] \tag{2}$$

where *I* and *m* are the discharge current and active material mass, respectively. While Δ*V* and Δt are operating potential as well as discharge time of the electrode.

The single electrode specific capacitance, $C_{sp}$ of the symmetric *SC* as a function of the specific current of the device was evaluated via the slope of the discharge profile in agreement with equation 3 as stated below [33]:

$$C_{sp} = \frac{4I \times \Delta t}{m \times \Delta V} \quad [F g^{-1}] \tag{3}$$

The energy density ($E_d$) basically expressed in J $g^{-1}$ and its equivalent power density ($P_d$) for the cell were evaluated from relations (4) and (6):

$$E_d = 0.5 C_s (\Delta V)^2 \tag{4}$$

The expression in Eq. 4 above was divided by a factor of 3600 to transform its units from J $g^{-1}$ to W h $g^{-1}$. The expression was further multiplied by a factor of 1000 to have the required units in W h $kg^{-1}$ as illustrated below:

$$E_d = 0.5C_s(\Delta V)^2 = \frac{1000 \times \mathrm{C}(\Delta \mathrm{V})^2}{2 \times 4 \times 3600}$$

Thus, the energy and power densities are expressed as:

$$E_d = \frac{\mathrm{C} \cdot \Delta V^2}{28.8} \ [\mathrm{Wh\ k}g^{-1}] \quad (5)$$

$$P_d = 3.6 \times E_d/\Delta t \quad [\mathrm{Kw\ kg^{-1}}] \quad (6)$$

where $E_d$ and $P_d$ *are* energy and power densities respectively.

The columbic efficiency, $C_E$ over a potential, *V* (V), of the symmetric *SC* was estimated using the following relation:

$$C_E = \frac{C_{sd}}{C_{sc}} \times 100\% \quad (7)$$

where $C_{sc}$ and $C_{sd}$, and $C_E$ (%) are specific capacitances of charge and discharge process, as well as the coulombic efficiency respectively.

## RESULTS AND DISCUSSION

### Formation and morphological characterization

The formation process of the high porosity ASCs with KOH is as a result of gasification of the carbon by removing $CO_2$ gas, and the oxygen material that is present in the matrix. During activation, $CO_2$ gas formed due to decomposition of $K_2CO_3$ during calcination is

liberated and becomes notable at elevated temperatures. This liberated $CO_2$ subsequently reacted with the hydrochar of the dehydrated sugar to activate dormant pores and liberate existing micropores. Alternatively, the $K_2CO_3$ can be reduced by carbon to generate metallic potassium (K), resulting in the carbon gasification and thus, pores formation. The below reaction depicts the activation process [31,32]:

$$6KOH + 2C \leftrightarrow 2K + 3H_2 + 2K_2CO_3 \quad (8)$$

Figure 1 (a-d) reveals the SEM images of ASCs materials. From the figure, it is clearly observed that the KOH activation results in formation of cavities [32], with the presence of large amount of pores in the 3D interconnection closely linked within the materials' structures. The fine structure was observed to be distorted at higher activation temperature (Fig. 1(d)).

Figure 2 (a-d) shows the TEM micrographs of the as-prepared ASCs materials at a magnification of 1 µm for ASC 400, 500, 600 and 700 respectively. It can be noticed that all as-prepared carbon samples display a porous morphology with the varying pore sizes attributed to the activation process originating within the material structure, which is further confirmed by the SEM micrographs shown in Fig. 1. A porous cavity of this nature could enhance charge storage mechanism by allowing easy ion penetration from the electrolyte into the various active sites within the material thereby enhancing the electrochemical properties of the material [2].

Fig. 3(a and b) displays the textural attributes of the ASCs samples analyzed using the $N_2$ adsorption/desorption isotherm measurements, which is further confirmed by the SEM micrographs shown in Fig. 1.

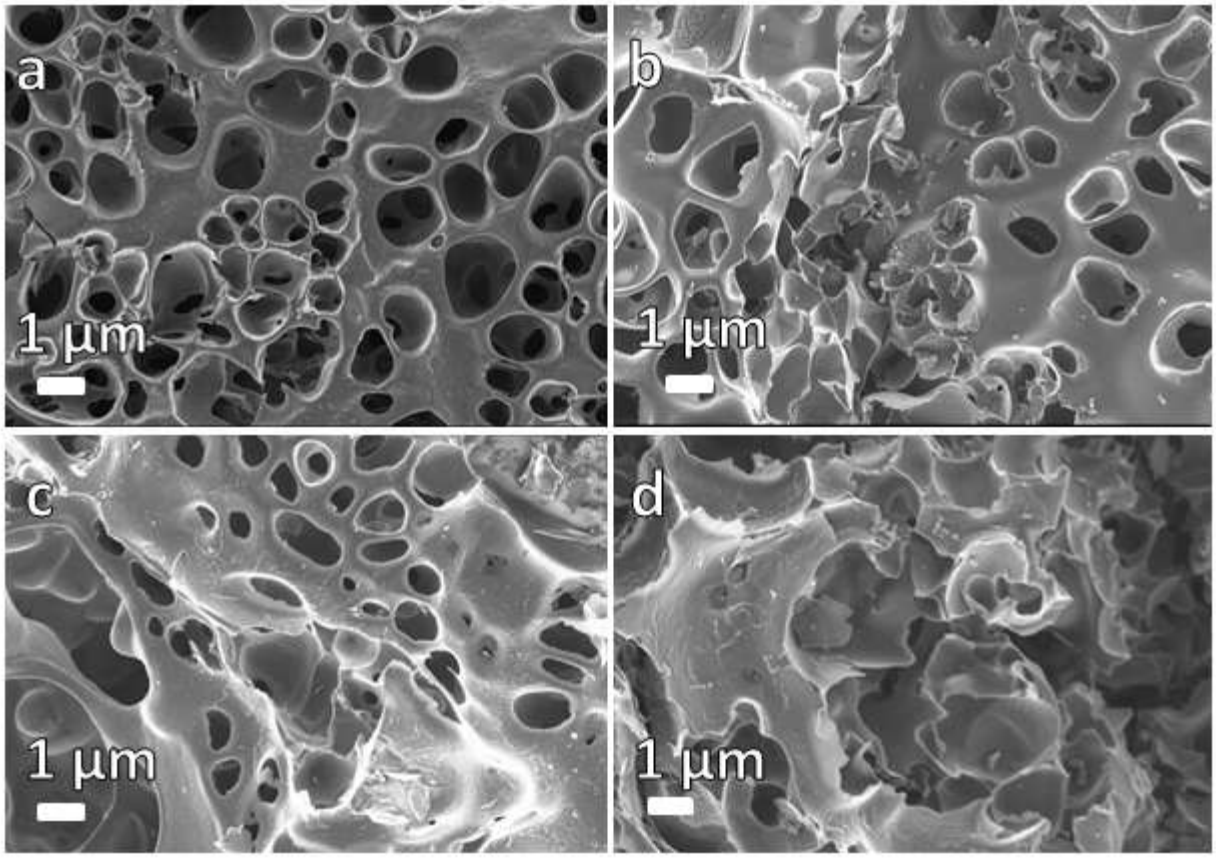


**Fig. 1:** SEM images of (a) ASC 400, (b) ASC 500, (c) ASC 600, and (d) ASC 700 respectively.

Fig. 3(a) exhibits that all the samples portray a type-II behavior, with H4-type hysteresis, showing complex materials comprising both mesopores and micropores [34]. Fig. 3(b) reveals the pore-size distribution (PSD) graphs of as-prepared materials, indicating the presence of mesopores within the structure of the materials. The PSD results further confirms the noticed results from the $N_2$ gas-sorption isotherm displayed in Fig. 3(a).

The higher surface area of the ASCs samples as well as the PSD could be advantageous in storing charges by the provision of noble adsorbate accessibility with larger flow paths to micropores [32,35].

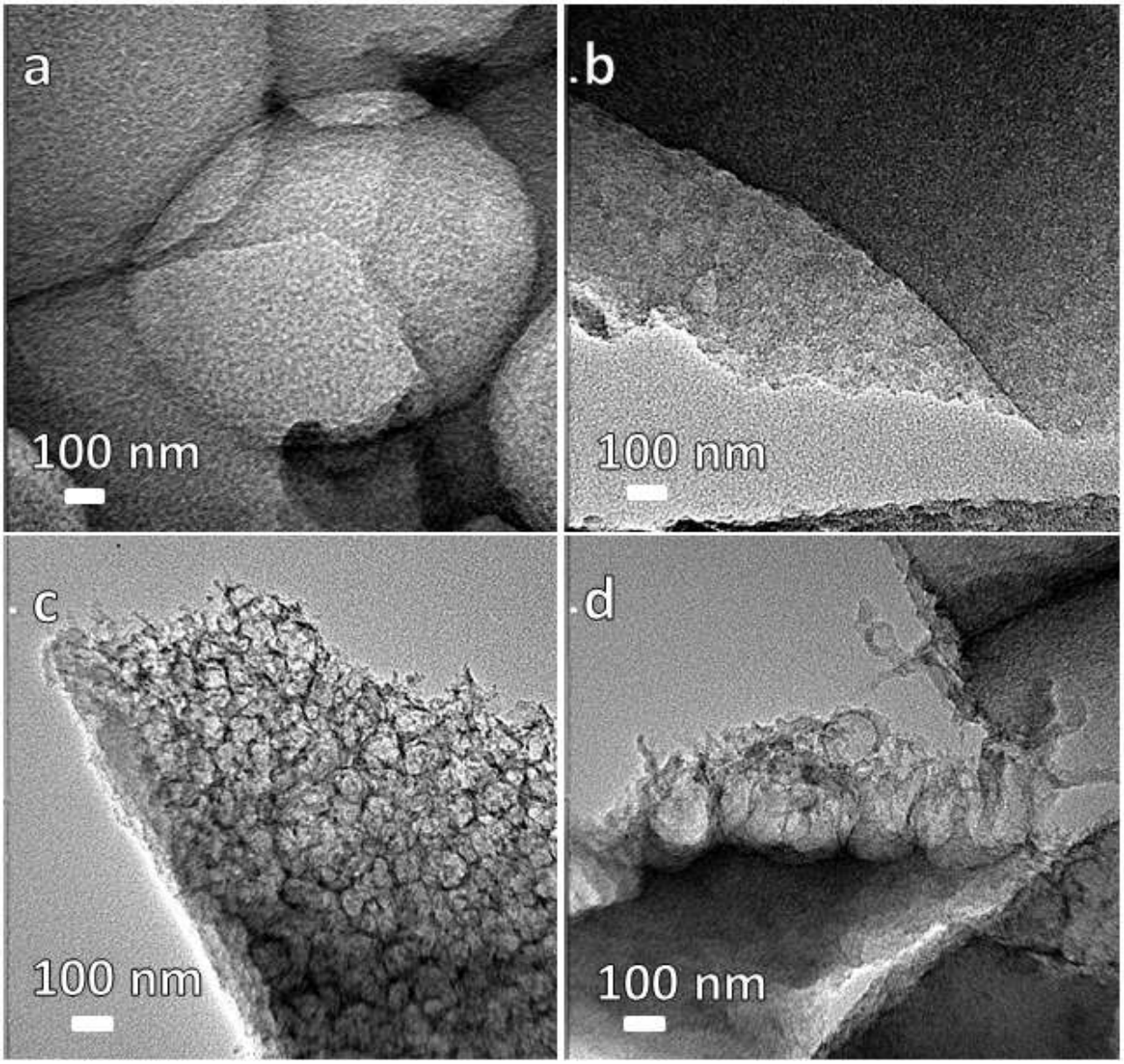


**Fig. 2:** TEM micrographs of (a) ASC 400, (b) ASC 500, (c) ASC 600, and (d) ASC 700 respectively.

Table 1 shows a summary of the results from BET analysis. The pore volume was observed to increase with increasing temperature (except for ASC 500) used during activation steps. ASC 400 with the second highest SSA (713.1171 $m^2 g^{-1}$) and 0.1712 $cm^3$ micropore volume is preferable for supercapacitor application. This is ascribed to its larger specific capacitance as well as better stability compared to other samples in 1 M $Na_2SO_4$ electrolyte (*see Fig. 6*).

**Table 1:** Physical properties of ASC 400, ASC 500, ASC 600 and ASC 700 obtained by KOH activated carbon derived from white granulated sugar.

| Samples | BET SSA, $m^2\ g^{-1}$ | Total pore volume, $cm^{-3}$ | Micropore volume, $cm^{-3}$ |
|---|---|---|---|
| **ASC 400** | 713.1171 | 0.4451 | 0.1712 |
| **ASC 500** | 234.1785 | 0.1491 | 0.1045 |
| **ASC 600** | 681.8927 | 0.4459 | 0.3329 |
| **ASC 700** | 1006.1411 | 0.6340 | 0.4662 |

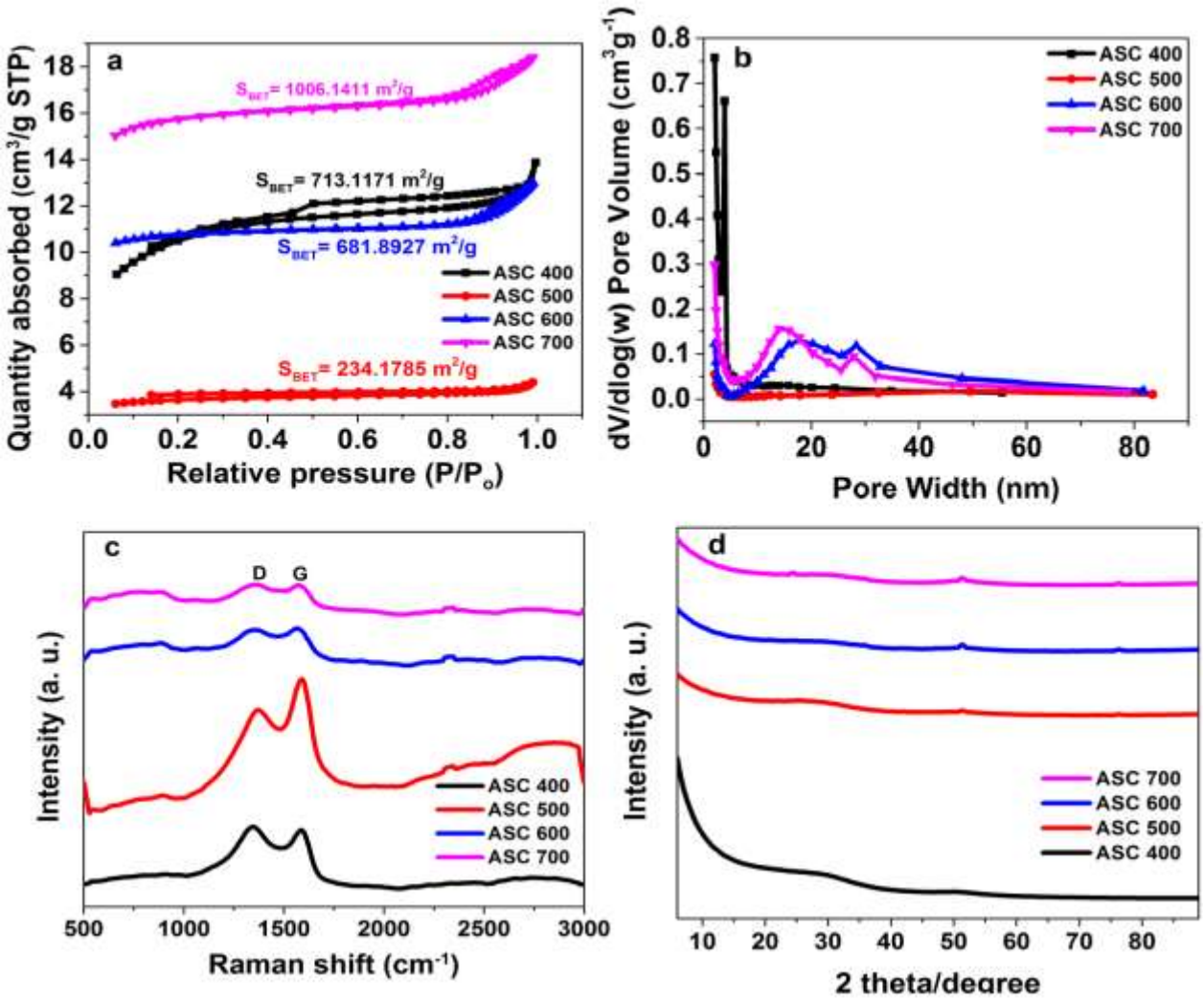


**Fig. 3:** (a) $N_2$ isotherms, (b) Pore size distribution, (c) Raman spectra, and (d) X-ray diffraction patterns of ASC 400, ASC 500, ASC 600, and ASC 700 samples respectively.

Figure 3(c) shows the representative Raman analysis of as-prepared ASCs. The D band at ~1373 $cm^{-1}$ indicates a disordered carbon, which resulted from the pausing modes of $sp^2$ rings actuated via a pair of resonance effects within the immediate proximity of defects. A G band observed at around ~1590 $cm^{-1}$ is due to the in-plane stretching phonon mode of C to C bond in the graphitized materials. The broad 2D band at around ~2700 $cm^{-1}$ is ascribed to the two-phonon lattice resonance. This 2D band is a typical of graphitic carbon [36,37]. The high intensity of the D-band and the broad 2D band portrayed in the spectra is ascribed to a fairly large amount of defects that is present of in the samples. The intensity ratio, D peak to G peak ($I_D/I_G$) is adopted to establish the degree of crystallization or density of defects in the carbon materials. The estimated $I_D/I_G$ are 0.85, 0.86, 0.86 and 0.86, for ASC 400, ASC 500, ASC 600 and ASC 700 samples, respectively, confirming the as-prepared samples amorphous nature [37].

Fig. 3(d) presents a representative XRD pattern of all ASCs samples. It can be observed that all the samples show comparable XRD patterns, with peaks identified with graphite materials. All the samples are amorphous in nature displaying broad diffraction peaks near a 2θ-value of 27 and 51, attributed to typical (002) and (101) planes of graphitic carbon (JCPDS no. 41-1487).

## Electrochemical measurements

*Standard three-electrode evaluations of single electrodes*

To study the ideal working condition and electrochemical behaviour of the as-prepared electrode materials, a three-electrode set-up was employed using a neutral 1M $Na_2SO_4$ aqueous electrolyte.

Fig. 4(a) and (b) show CV and CD curves of as-prepared samples at a scan rate and a specific current of 50 mV $s^{-1}$ and 0.5 A $g^{-1}$ respectively, evaluated in 1 M $Na_2SO_4$ aqueous electrolyte. From Fig. 4(a), a quasi-rectangular CV curve was observed for all the samples, an ideal electrical double layer capacitor (EDLC) nature. The quasi-rectangular CV curves indicate a swift electrochemical response, confirming a satisfying electrical conductivity of the samples in 1 M $Na_2SO_4$, and a demonstration of the formation of a double layer mechanism [32,38]. A higher charge separation was observed for the ASC 400 compared to the other samples, which also displays a pore volume of 0.4451 $cm^{-3}$. Fig. 4(b) exhibits a quasi-symmetrical triangular CD curves for all the ASCs, confirming the EDLC characteristics observed in CV curves shown in Fig. 4(a). The ASC 400 sample is of interest since it shows better electrochemical properties regardless of being second to the other sample (ASC 700) in terms of SSA. Hence, detailed study is done on this sample. Fig. 4(c) presents the CV curves of the as-prepared ASC 400 both in negative and positive operating potentials, ranging from -0.8 V to 0.8 V. The figure shows that the material could operate well in a reversible operating potential.

Fig. 5(a) and (b) show the detailed electrochemical response of the ASC 400 half-cell electrode with the characteristic CV and CD curves tested at distinct scan rates, and specific currents ranging from 10 to 100 mV $s^{-1}$, and 0.5 to 5 A $g^{-1}$ in 1 M $Na_2SO_4$ electrolyte, respectively. The less distorted CV and CD curves observed for the sample display the swift ion diffusion kinetics as well as rapid current response on potential reversal of the sample electrode [39]. The well-saturated porous structure of the electrode material by the electrolyte, allows the ions to be readily available at the electrode/electrolyte interface. The ions are attracted and pushed off from the electrode over a short distance, thereby providing direct and rapid ion transport pathways [38-39,40,48].

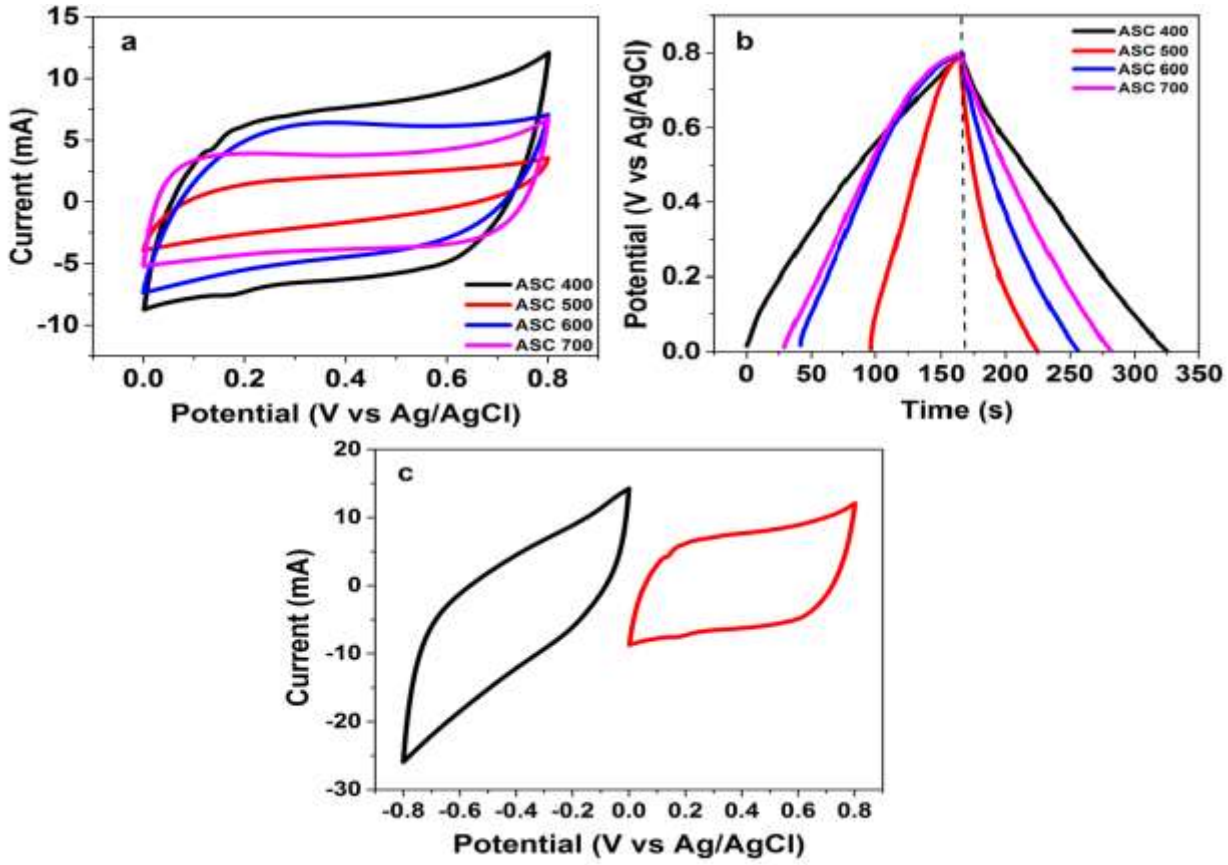


**Fig. 4.** (a) CV curves, and (b) CD curves of all ASCs at a specific current of 0.5 A $g^{-1}$ and a scan rate of 50 mV $s^{-1}$ in 1 M $Na_2SO_4$ respectively. (c) CV curves of ASC 400 at both negative and positive potentials.

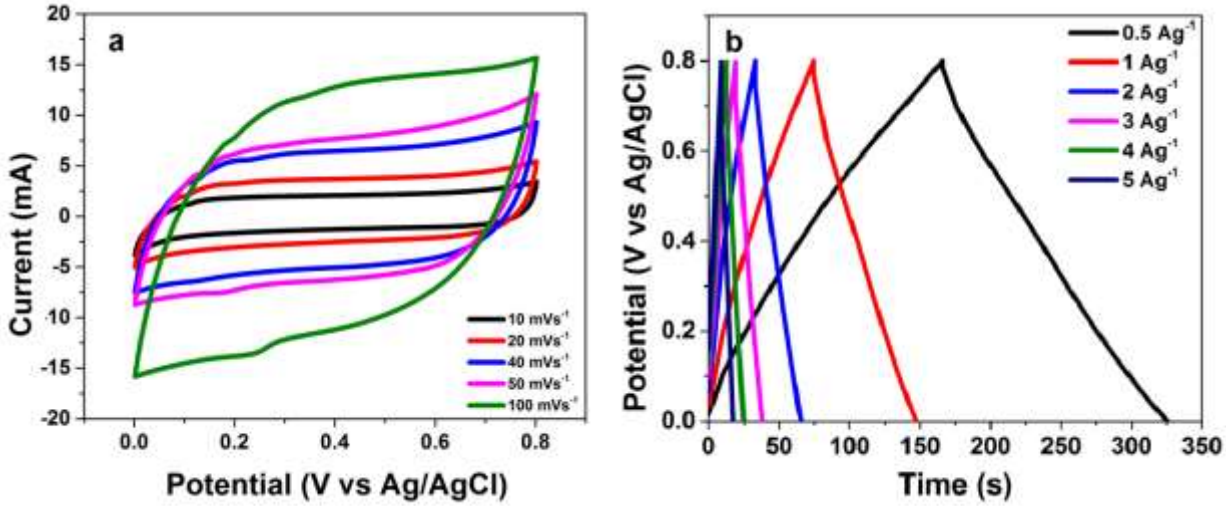


**Fig. 5.** (a) CV curves at different specific currents, and (b) CD curves of ASC 400 at distinct scan rates respectively.

Fig. 6 (a) depicts the radar plot of specific capacitances of all the ASCs samples evaluated in line with equation 2 and plotted with respect to specific currents. From the Figure, ASC 400 electrode was noticed to display a maximum specific capacitance of 100.8 F $g^{-1}$, which could be attributed to its moderate pore cavities resulting in good surface reactivity of the material with the electrolyte's $OH^-$ groups. The ASC 500, ASC 600 and ASC 700 samples show a specific capacitance value of 37.5, 56.88, and 72.69 F $g^{-1}$ at a specific current of 0.5 A $g^{-1}$, respectively. Fig. 6 (b) displays a full plot of specific capacitance at different specific currents for the as-prepared ASC 400 electrode. The electrode material could yield specific capacitance values of 108.8, 93.8, 85.0, 78.8, 67.5, and 62.5 F $g^{-1}$ at specific currents of 0.5, 1.0, 2.0, 3.0, 4.0, and 5 A $g^{-1}$ respectively between 0 V and 0.8 V working potential range.

Fig. 6(c) shows the specific capacitance retention, while Fig. 6(d) presents the coulombic efficiency of an ASC 400 electrode plotted against the cycle number for over 2000 CD cycles. A capacitance retention value of approximately 85.2% (see Fig. 6(c)) was retained, with a corresponding coulombic efficiency of about 98.53% (see Fig. 6(d)) for the single electrode. The high capacitance retention displayed by the sample could be attributed to a high ionic conductivity, as a result of the porous structure that avail the material to be largely more accessible for ion diffusion within the pores of the 3D interconnection linked together in the materials' frameworks [40,41].

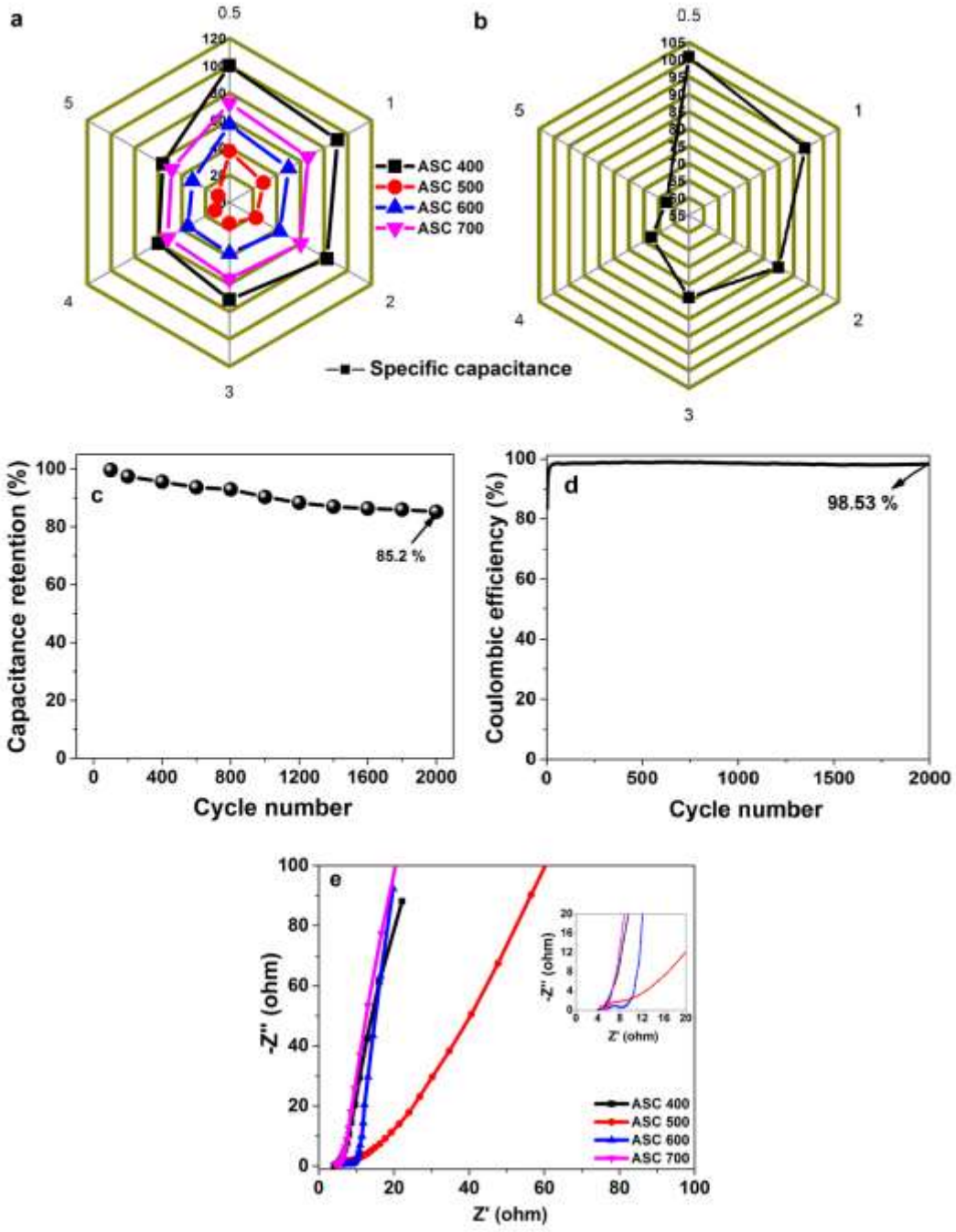


**Fig. 6.** (a) Plot of specific capacitances against specific currents for all ASCs electrodes, (b) a plot of specific capacitances against specific currents for ASC 400 electrode, (c) percentage capacitance retention, (d) coulombic efficiency for ASC 400 electrode against the cycle number performed at 3 A $g^{-1}$, and (e) Nyquist impedance plots of all the ASCs electrodes.

Besides, the electrochemical reactions typically rely on the insertion-extraction of $OH^-$ from the electrolyte. More-over, the porous structure is advantageous for the ions diffusion into holes of the electrode [40,41].

The electrical resistance of the ASCs electrodes was further evaluated by investigating the electrochemical impedance spectroscopy (EIS) at an open circuit potential (OCP) of 0.0 V and a frequency, ranging from 10 mHz - 100 kHz. Fig. 6(e) portrays the Nyquist plots of all ASCs samples in 1 M $Na_2SO_4$. It is worth observing that the Nyquist plots display distinct semicircle in the high-frequency regions (see insets to Fig. 6(e)), an attribute of the interfacial charge transfer resistance and mass transport through the materials.

The intersection of Nyquist plot and the horizontal axis, describes the sum resistance resulting from the addition of ionic resistance of the electrolyte, intrinsic resistance of the active materials and the contact resistance between the active electrode material/current collector interface [42], designated as $R_S$. In Fig. 6(e), $R_S$ values are estimated to be approximately 3.8 Ω, 5.4 Ω, 5.3 Ω and 4.4 Ω for ASC 400, 500, 600 and 700 respectively. The $R_S$ for ASC 400 was observed to be smallest, which is responsible for the material's better electrochemical performance. This is due to the material's short diffusion length linked to the fine size of the pores [42,48].

*Electrochemical measurements of the symmetric ASC 400 supercapacitor*

As a result of the remarkable stability of ASC 400 electrode material, a symmetric supercapacitor, *SC* was fabricated. The sum specific mass loading of active materials in the symmetric *SC* electrodes was determined to be about 4.0 mg $cm^{-2}$ via a digital weighing balance. Electrochemical evaluation of the symmetric *SC* was done in a two-

electrode set-up in 1 M $Na_2SO_4$, based on the better electrochemical performance demonstrated from the half-cell analysis.

Fig. 7(a) shows the CV curves of symmetric ASC 400//ASC 400 device measured at distinct scan rates between 5 to 100 mV $s^{-1}$. Fig. 7(b) shows the associated CD profiles of the full device at various gravimetric current densities. The CV and CD curves are observed to be fairly rectangular and symmetrical respectively, which is in accordance with the EDLC nature of activated carbon symmetric devices [30,32,39,43]. Fig. 7(c) displays the specific capacitance of the symmetric *SC* estimated by using equation 3, and plotted against the gravimetric specific current.

At a specific current of 1.0 A $g^{-1}$, the *SC* was observed to produce a maximum specific capacitance of 242.67 F $g^{-1}$. Fig. 7(d) depicts a Ragone plot for both energy and power densities which are two decisive variables used in estimating the potential electrochemical suitability for real life applications. These variables were obtained for the device in accordance with equations 5 and 6, resulting in an energy density of about 19 Wh $kg^{-1}$, giving rise to an equivalent power density of 750.0 W $kg^{-1}$ at a specific current of 1.0 A $g^{-1}$, respectively. The energy density and specific capacitance displayed by the *SC* proved considerable progress compared to some other sugar-derived symmetric *SCs* using aqueous electrolyte [23,44,45].

In Fig. 7(e), it was seen that the *SC* highlights a superb coulombic efficiency of nearly 100 % determined in line with equation 7, and as well, conserves up to 88.2% of its initial capacitance for over 10000 cycles at a specific current of 3.0 A $g^{-1}$. A characteristic ascribed to the fine porous structure, which plays a major role in heightening the efficient electrode surface area, and thereby facilitating electrolyte permeation. Therefore, shortening the electron pathways within the active materials [46,48]. Fig. 7(f) displays the

position of the device in this work in terms of energy and power densities. The chart in Fig. 7(f) reveals that the values obtained for our symmetric ASC 400 device are considerably better compared to some other sugar-based supercapacitors from literature.

EIS technique was further employed to determine the electrochemical performance of the symmetric *SC*, and is depicted in Fig. 8(a-c). Fig. 8(a) portrays the Nyquist plot, and a fit utilizing the equivalent circuit. From the circuit, a solution resistance, $R_s$ and a charge transfer resistance, $R_{CT}$ were calculated to be nearly 0.83 Ω and 0.13 Ω, respectively. A considerably smaller value compared with what was reported for some similar materials in literature [30,44]. This implies the desirable electrical behaviours of the material adopted in the symmetric *SC*.

Furthermore, the Nyquist plot of the symmetric ASC 400 *SC* was fitted as seen in Fig. 8(a) using a ZFIT fitting program with an associated equivalent circuit. In the circuit, $R_S$ is connected in series with two other units. $Q_1$ is in parallel with the charge transfer resistance, $R_{CT}$, which is situated serially with the constant phase element $Q_2$ that is connected parallel to the leakage resistance $R_L$.

A Warburg diffusion element designated as *W*, modeled the transition from a high frequency to a low frequency region, and is connected in series with $R_{CT}$. The estimated magnitudes of $R_s$, $R_{CT}$, $R_L$, and Q utilizing a ZFIT program software are presented in Table 2. The symmetric *SC* however, reveals a deviation from the ideal *SC* behaviour due to a resistive element, $R_L$ associated and connected parallel with $Q_2$.

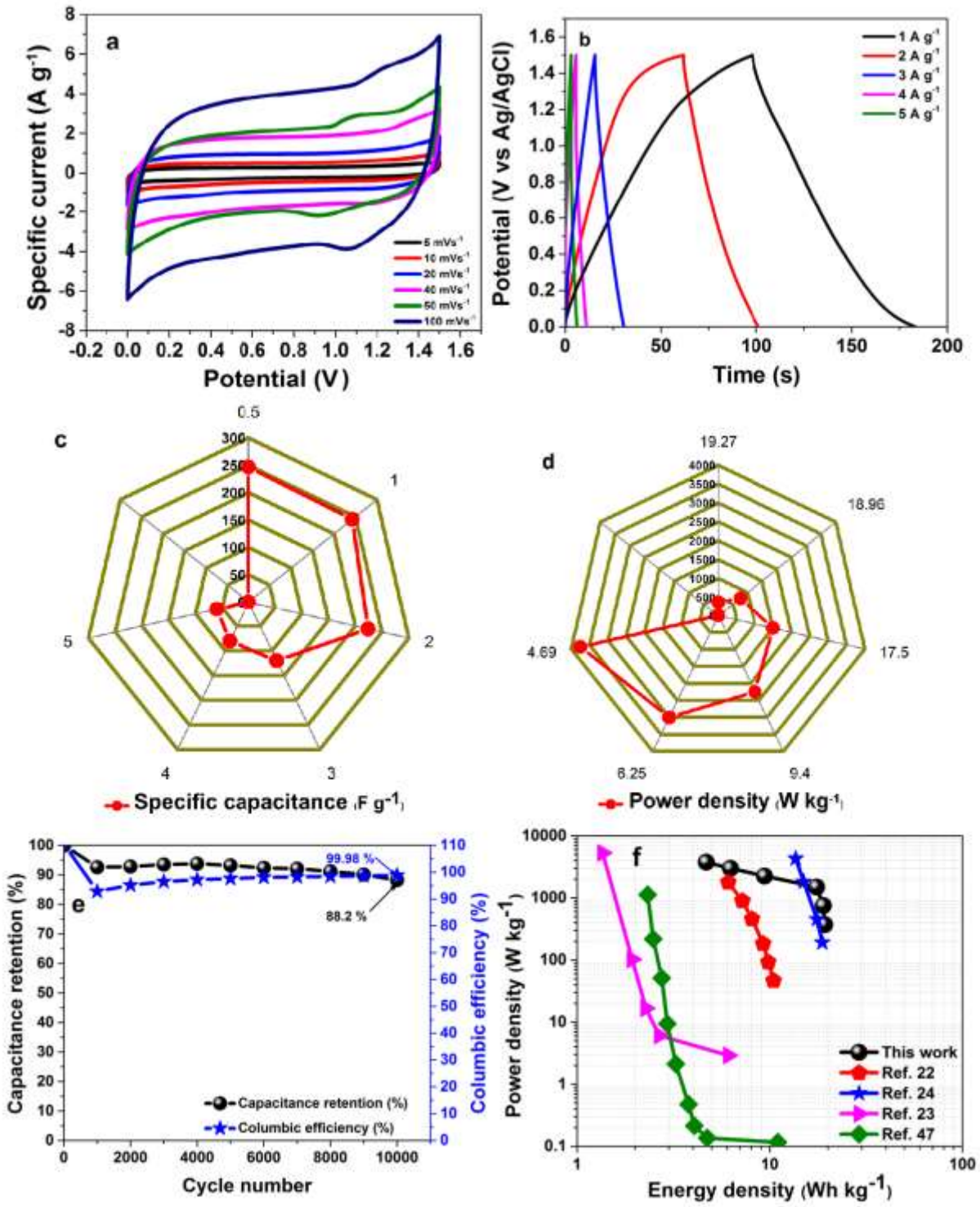


**Fig. 7.** (a) CV curves at distinct scan rates, (b) CD curves at various specific currents, (c) specific capacitance determined at various specific currents, (d) Ragone plots, and (e) cyclic performances of the symmetric ASC 400 device. (f) Ragone chart of the device, with some other sugar-based material electrodes recently reported from the literature.

**Table 2**: Calculated magnitudes of $R_s$, Q, $R_{CT}$, $R_L$, and $A$ (Warburg coefficient) fitted parameters via a ZFIT fitting of the experimental impedance spectra in line with the equivalent circuit depicted in the Fig. 8(a).

| **Electrode** | **$R_s$ (Ω)** | **$Q_1$ ($F.s^{(a-1)}$)** | **$A_1$** | **$R_{CT}$ (Ω)** | **$Q_2$ ($F.s^{(a-1)}$)** | **$A_2$** | **$R_L$ (Ω)** |
|---|---|---|---|---|---|---|---|
| **ASC 400** | **0.832** | **0,042** | **0.937** | **4.201** | **0,060** | **0.3** | **457** |

**$X^2 = 0.11$; $X/N^{1/2} = 1.107$; a ≡ n.**

Fig. 8(b) shows the nature of the CV curves for the ASC 400 symmetric device before and after being subjected to over 10000 CD cycles at a 50 mV $s^{-1}$ scan rate. It can be observed that after the cycling test, the device current response slightly decreased, which is a correlation of an increase in resistance. This is shown by increase in radius of the semicircle in the high frequency region, as observed in Fig. 8(c). In Fig. 8(c), the $R_{CT}$ calculated using a Circular Fit Bio-Logic software, was seen to have increased from the initial 0.13 Ω to 2.3 Ω over a 10000 CD cycling test.

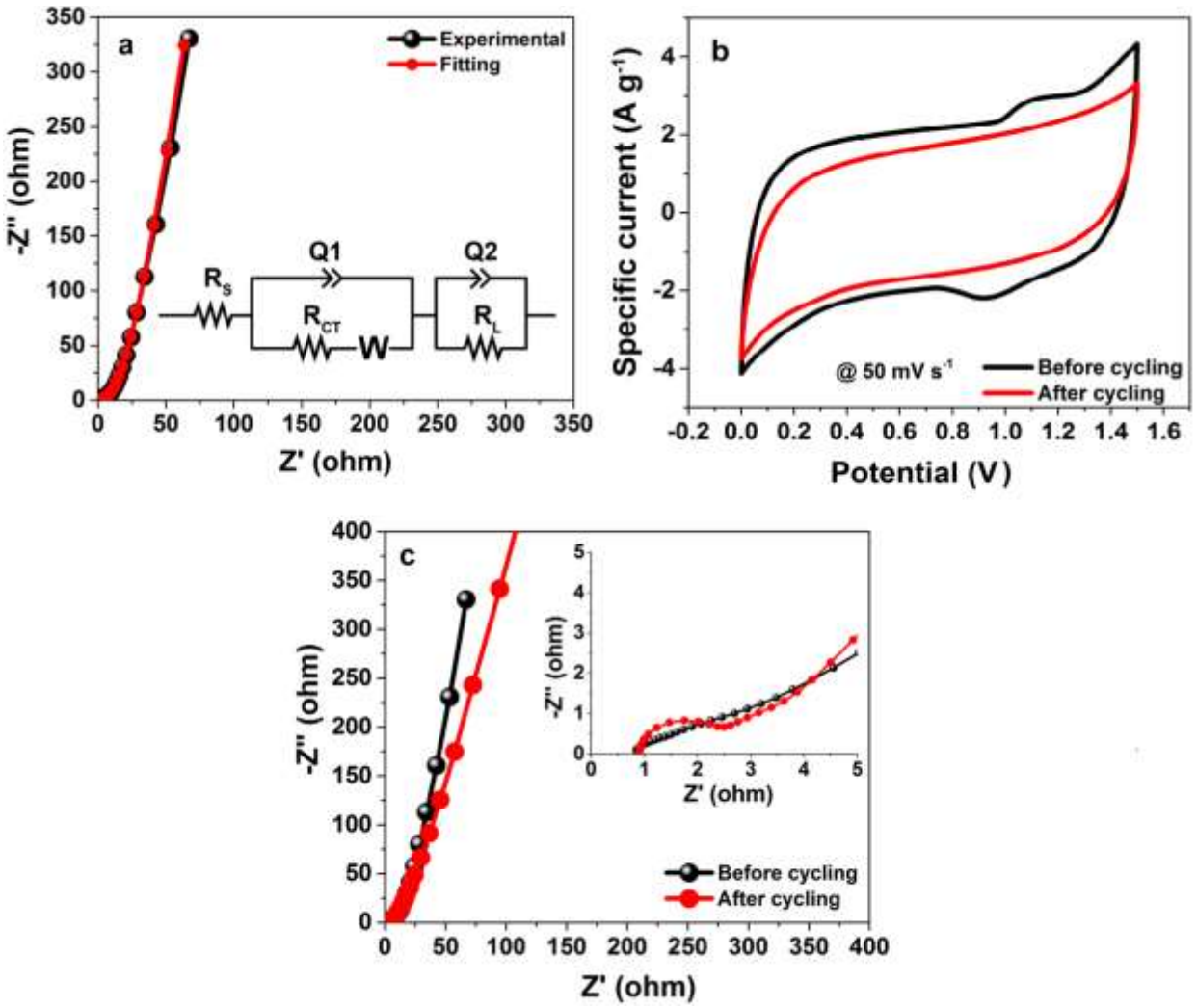


**Fig. 8.** (a) EIS and fitting curves, (b) CV profiles before and after cycling test for the symmetric *SC*, respectively and (c) EIS before and after 10000 cycling of the symmetric *SC* at a specific current of 3 A $g^{-1}$.

## CONCLUSION

In this work, we have successfully synthesized and characterized sugar-based activated carbon (ASC) material using a facile two-step synthesis method. Diverse material characterization of the as-synthesized ASC sample depicted a porous morphology with high specific surface area (SSA) in the order of 713.12, 234.18, 681.89, and 1006.14 $m^2$ $g^{-1}$ for ASC 400, ASC 500, ASC 600, and ASC 700, respectively. The ASC 400 sample

stands out owing to its better electrochemical properties as compared to the other samples. A promising electrochemical behaviour was also demonstrated in terms of the assembled symmetric device which revealed a maximum specific capacitance value of 242.67 F $g^{-1}$ with a corresponding energy and power densities of nearly 19 Wh $kg^{-1}$ and 750 W $kg^{-1}$ respectively at a 1 A $g^{-1}$ specific current. This was obtained by optimizing the operating electrolyte with the 1 M $Na_2SO_4$ electrolyte supplying enhanced electrochemical response within a working potential window of 1.5 V. The material shows no considerable capacitance loss (11.8 %) up to 10000 cycling at a specific current of 3 A $g^{-1}$.

The facile few-step synthesis procedure adopted in the study is cost-effective and sustainable compared to other organic and inorganic sources. Our results suggest the potential for adopting this material in developing high performance energy storage devices with room for greater advancement, with further research growth on ASC-based materials in aqueous electrolytes for enhanced electrochemical performance supercapacitor applications.

## ACKNOWLEDGEMENTS

This research is based on the sponsorship of the South African Research Chairs Initiative of the Department of Science and Technology and National Research Foundation of South Africa under grant number: 61056. The authors thank the University of Pretoria and National Research Foundation (NRF) for studentship grants.

## REFERENCES


1. Miller, J. R. & Simon, P. Materials science. Electrochemical capacitors for energy management. *Science* **2008**, 321, 651–652, DOI 10.1126/science.1158736.

2. Simon, P. & Gogotsi, Y. Materials for electrochemical capacitors. *Nat. Mater.* **2008,** 7, 845–854, DOI 10.1038/nmat2297.

3. Barzegar, F., *Bello, A., Guellati, O., Momodu, D.Y., Harat, A., Dangbegnon, J.K., Guerioune, M., Manyala N.* Effect of addition of different carbon materials on hydrogel derived carbon material for high performance electrochemical capacitors. *Electrochim. Acta* **2015**, *186,* 277-284, DOI 10.1016/j.electacta.2015.10.189.

4. Huang, Y. *Li, Y., Hu, Z., Wei, G., Guo, J., Liu, J.* A carbon modified MnO2 nanosheet array as a stable high-capacitance supercapacitor electrode. *J. Mater. Chem. A* **2013,**1, 9809–9813, DOI 10.1039/c3ta12148h.

5. Lu, M. Supercapacitors Materials, Systems and Applications. John Wiley & Sons: Weinheim, **2013**.

6. Wang, X. *Kajiyama, S., Iinuma, H., Hosono, E., Oro, S., Moriguchi, I., Okubo, M., Yamada, A.* Pseudocapacitance of MXene nanosheets for high-power sodium-ion hybrid capacitors. *Nat. Commun.* **2015**, 6, 1-6, DOI 10.1038/ncomms7544.

7. Barzegar, F. Synthesis and characterization of activated carbon materials for supercapacitor applications. PhD Thesis, University of Pretoria, **2016**.

8. Stoller, M. D., Park, S., Yanwu, Z., An, J. & Ruoff, R. S. Graphene-Based ultracapacitors. *Nano Lett.* **2008**, 8, 3498–3502, DOI 10.1021/nl802558y.

9. Momodu, D. *Bello, A., Oyedotun, K., Ochai-Ejeh, F., Dangbegnon, J., Madito, M., Manyala, N.* Enhanced electrochemical response of activated carbon nanostructures from tree-bark biomass waste in polymer-gel active electrolytes. *RSC Adv.* **2017**, 7, 37286-37295, DOI 10.1039/c7ra05810a.

10. Conway, B.E. Electrochemical supercapacitors: scientific fundamentals and technological applications. Springer Science & Business Media: New York, **2013**.

11. Lee, B. G. & Lee, S. H. Application of hybrid supercapacitor using granule $Li_4Ti_5O_{12}$/activated carbon with variation of current density. *J. Power Sources* **2017**, 343, 545–549, DOI 10.1016/j.jpowsour.2017.01.094.

12. Lee, S. H. & Kim, J. M. Punched $H_2Ti_{12}O_{25}$ anode and activated carbon cathode for high energy/high power hybrid supercapacitors. *Energy* **2018**, 150, 816–821, DOI 10.1016/j.energy.2018.03.038.

13. Choi, H. J., Lee, S. H., Kim, J. H., Kim, H. K. & Kim, J. M. Zinc doped $H_2Ti_{12}O_{25}$ Anode and Activated Carbon Cathode for Hybrid Supercapacitor with superior performance. *Electrochim. Acta* **2017**, 251, 613–620, DOI 10.1016/j.electacta.2017.08.094.

14. Lee, S. H., Kim, J. H. & Yoon, J. R. Laser Scribed Graphene Cathode for Next Generation of High Performance Hybrid Supercapacitors. *Sci. Rep.* **2018**, 8, 1–9, DOI 10.1038/s41598-018-26503-4.

15. Sun H., Xu Z., and Gao C. Multifunctional, ultra-flyweight, synergistically assembled carbon aerogels. Advanced Materials **2013**, 25, 2554–2560, DOI 10.1002/adma.201204576.

16. Wang, R., Sui, Y., Huang, S., Pu, Y. & Cao, P. High-performance flexible all-solid-state asymmetric supercapacitors from nanostructured electrodes prepared by oxidation-assisted dealloying protocol. *Chem. Eng. J.* **2018**, 331, 527–535, DOI 10.1016/j.cej.2017.09.004.

17. Liu, X., Wei, F., Sui, Y., Qi, J., He, Y., & Meng, Q.Polyhedral ternary oxide $FeCo_2O_4$: A new electrode material for supercapacitors. *J. Alloys Compd.* **2018**, 735, 1339–1343, DOI 10.1016/j.jallcom.2017.11.251.

18. Qi, J., Chang, Y., Sui, Y., He, Y., Meng, Q., Wei, F., Ren, Y. and Jin, Y. Facile Synthesis of Ag-Decorated $Ni_3S_2$Nanosheets with 3D Bush Structure Grown on rGO and Its Application as Positive Electrode Material in Asymmetric Supercapacitor. *Adv. Mater. Interfaces* **2018**, 5, 1–9, DOI 10.1002/admi.201700985.

19. Ma, G. *Yang, Q., Sun, K., Peng, H., Ran, F., Zhao, X., Lei, Z.* Nitrogen-doped porous carbon derived from biomass waste for high-performance supercapacitor. *Bioresour. Technol.* **2015**, 197, 137–142, DOI 10.1016/j.biortech.2015.07.100.

20. Abioye, A. M. & Ani, F. N. Recent development in the production of activated carbon electrodes from agricultural waste biomass for supercapacitors: A review. *Renew. Sustain. Energy Rev.* **2015**, 52, 1282–1293, DOI 10.1016/j.rser.2015.07.129.

21. Rufford, T. E., Hulicova-Jurcakova, D., Zhu, Z. & Lu, G. Q. Nanoporous carbon electrode from waste coffee beans for high performance supercapacitors. *Electrochem. commun.* **2008**, 10, 1594–1597, DOI 10.1016/j.elecom.2008.08.022.

22. Rufford, T. E., Hulicova-Jurcakova, D., Khosla, K., Zhu, Z. & Lu, G. Q.

Microstructure and electrochemical double-layer capacitance of carbon electrodes prepared by zinc chloride activation of sugar cane bagasse. *J. Power Sources* **2010**, 195, 912–918, DOI 10.1016/j.jpowsour.2009.08.048.

23. Wahid, M., Puthusseri, D., Phase, D. & Ogale, S. Enhanced capacitance retention in a supercapacitor made of carbon from sugarcane bagasse by hydrothermal pretreatment. *Energy and Fuels* **2014**, 28, 4233–4240, DOI 10.1021/ef500342d.

24. Hao, P. *Zhao, Z., Tian, J., Li, H., Sang, Y., Yu, G., Cai, H., Liu, H., Wong, C.P., Umar, A.* Hierarchical porous carbon aerogel derived from bagasse for high performance supercapacitor electrode. *Nanoscale* **2014**, 6, 12120–12129, DOI 10.1039/C4NR03574G.

25. Lock, S. The Cambridge world history of food. *Med Hist* **2002**, 46, 267–270, DOI 10.1353/jwh.2003.0033.

26. Galloway, J. H. The Sugar Cane Industry. An Historical Geography from its Origins to 1914. *J. Chem. Inf. Model.* **2013**, 53, 1689–1699, DOI 10.1017/CBO9781107415324.004.

27. Flynn K., India Drought 2016 May Lead 29-35% Drop In Sugar Output For 2016-17 Season: Report, April 23, **2016**.

28. Rolph, G. M. Something about sugar; its history, growth, manufacture and distribution. Newbegin, John J.: San Francisco, **1917**.

29. Wang, Zhang, Y., Zhi, C., Wang, X., Tang, D., Xu, Y., Weng, Q., Jiang, X., Mitome, M., Golberg, D., Bando, Y. Three-dimensional strutted graphene grown by substrate-free sugar blowing for high-power-density supercapacitors. *Nat.*

*Commun.* **2013**, 4, 1–8, DOI 10.1038/ncomms3905.

30. Ma, J., Xue, T. & Qin, X. Sugar-derived carbon/graphene composite materials as electrodes for supercapacitors. *Electrochim. Acta* **2014**, 115, 566–572, DOI 10.1016/j.electacta.2013.11.028.

31. Chem, J. M., Wang, J. & Kaskel, S. FEATURE ARTICLE KOH activation of carbon-based materials for energy storage. **2012**, *22,* 23710–23725, DOI 10.1039/c2jm34066f.

32. Bello, A. *Manyala, N., Barzegar, F., Khaleed, A.A., Momodu, D.Y., Dangbegnon, J.K.* Renewable pine cone biomass derived carbon materials for supercapacitor application. *RSC Adv.* **2016**, 6, 1800–1809, DOI 10.1039/C5RA21708C.

33. Barzegar, F. *Khaleed, A.A., Ugbo, F.U., Oyeniran, K.O., Momodu, D.Y., Bello, A., Dangbegnon, J.K., Manyala, N.* Cycling and floating performance of symmetric supercapacitor derived from coconut shell biomass. *AIP Adv.* **2016**, 6, 115306-1, DOI 10.1063/1.4967348.

34. Kruk, M. & Jaroniec, M. Gas adsorption characterization of ordered organic-inorganic nanocomposite materials. *Chemistry of Materials* **2001**,13, 3169–3183, DOI 10.1021/cm0101069.

35. Pandolfo, A. G. & Hollenkamp, A. F. Carbon properties and their role in supercapacitors. *J. Power Sources* **2006**, 157, 11–27, DOI 10.1016/j.jpowsour.2006.02.065.

36. Pimenta, M. A. *Dresselhaus, G., Dresselhaus, M.S., Cançado, L.G., Jorio, A., Saito, R.* Studying disorder in graphite-based systems by Raman spectroscopy. *Phys.*

*Chem. Chem. Phys.* **2007**, 9, 1276–1290, DOI 10.1039/B613962K.

37. Sadezky, A. *Muckenhuber, H., Grothe, H., Niessner, R., Pöschl, U., Poschl, U.* Raman microspectroscopy of soot and related carbonaceous materials: Spectral analysis and structural information. *Carbon N. Y.* **2005**, 43, 1731–1742, DOI 10.1016/j.carbon.2005.02.018.

38. Fic, K., Lota, G., Meller, M. & Frackowiak, E. Novel insight into neutral medium as electrolyte for high-voltage supercapacitors. *Energy Environ. Sci.* **2012**, 5, 5842–5850, DOI 10.1039/C1EE02262H.

39. Zhou, J. *Zhu, T., Xing, W., Li, Z., Shen, H., Zhuo, S.* Activated polyaniline-based carbon nanoparticles for high performance supercapacitors. *Electrochim. Acta* **2015**, 160, 152–159, DOI 10.1016/j.electacta.2015.02.032.

40. Zhang, Y. *Ma, M., Yang, J., Su, H., Huang, W., Dong, X.* Selective synthesis of hierarchical mesoporous spinel NiCo(2)O(4) for high-performance supercapacitors. *Nanoscale* **2014**, 6, 4303–4308, DOI 10.1039/c3nr06564b.

41. Oyedotun, K. O. *Madito, M.J., Momodu, D.Y., Mirghni, A.A., Masikhwa, T.M., Manyala, N.* Synthesis of ternary NiCo-MnO 2 nanocomposite and its application as a novel high energy supercapattery device. *Chem. Eng. J.* **2018**, 335, 416–433, DOI 10.1016/j.cej.2017.10.169.

42. Liu, X. Y. *Zhang, Y.Q., Xia, X.H., Shi, S.J., Lu, Y., Wang, X.L., Gu, C.D., Tu, J.P.* Self-assembled porous NiCo2O4 hetero-structure array for electrochemical capacitor. *J. Power Sources* 239, **2013**, 157–163, DOI 10.1016/j.jpowsour.2013.03.106.

43. Lee, K. K. *Hao, W., Gustafsson, M., Tai, C.-W., Morin, D., Björkman, E., Lilliestråle, M., Björefors, F., Andersson, A.M., Hedin, N.*Tailored activated carbons for supercapacitors derived from hydrothermally carbonized sugars by chemical activation. *RSC Adv.* **2016**, 6, 110629–110641, DOI 10.1039/C6RA24398C.

44. Mahto, A. *Gupta, R., Ghara, K.K., Srivastava, D.N., Maiti, P., Kalpana, D., Zavala-Revira, P., Meena, R., Nataraj,S.K.* Development of high-performance supercapacitor electrode derived from sugar industry spent wash waste. *J. Hazard. Mater.* **2017**, 340, 189–201, DOI 10.1016/j.jhazmat.2017.06.048.

45. Wang, C., O'Connell, M. J. & Chan, C. K. Facile one-pot synthesis of highly porous carbon foams for high-performance supercapacitors using template-free direct pyrolysis. *ACS Appl. Mater. Interfaces* **2015**, 7, 8952–8960, DOI 10.1021/acsami.5b02453.

46. Chen, T. *Tang, Y., Qiao, Y., Liu, Z., Guo, W., Song, J., Mu, S., Yu, S., Zhao, Y., Gao, F.* All-solid-state high performance asymmetric supercapacitors based on novel MnS nanocrystal and activated carbon materials. *Sci. Rep.* **2016**, 6, 1-9, DOI 10.1038/srep23289.

47 Si, T., Zhou, J., Zhang, S., Li, S., Xing, W., Zhuo, S. Tunable N-doped or dual N, S-doped activated hydrothermal carbons derived from human hair and glucose for supercapacitor applications. Electrochim. Acta **2013**, 107, 397-405, DOI 10.1016/j.electacta.2013.06.065.

48 Barzegar, F., Zhang, L., Bello, A., Manyala N., and Xia X. Three dimensional modelling of the components in supercapacitors for proper understanding of the contribution of each parameter to the final electrochemical performance. J. Mater.

Chem. A, **2018**, 6, 17481–17487, DOI 10.1039/C8TA04736G.

## Table of Contents Synopsis

Novel and cost-effective porous carbon material was synthesized via acidic dehydration of white sugar for supercapacitor electrode applications.